City Research Online

City St George's, University of London

Citation: Aqel, O., White, M. & Sayma, A. (2024). Loss Analysis in Radial Inflow Turbines for Supercritical CO2 Mixtures. Journal of Turbomachinery, 146(5), 051003. doi: 10.1115/1.4064193

This is the published version of the paper.

This version of the publication may differ from the final published version. To cite this item please consult the publisher's version.

Permanent repository link: https://openaccess.city.ac.uk/id/eprint/32430/

Link to published version: https://doi.org/10.1115/1.4064193

Copyright and Reuse: Copyright and Moral Rights remain with the author(s) and/or copyright holders. Copies of full items can be used for personal research or study, educational, or not-for-profit purposes without prior permission or charge, unless otherwise indicated, provided that the authors, title and full bibliographic details are credited, a hyperlink and/or URL is given for the original metadata page and the content is not changed in any way. For full details of reuse please refer to City Research Online policy.

City Research Online: http://openaccess.city.ac.uk/ publications@citystgeorges.ac.uk

Check for updates

ASME Journal of Turbomachinery
Online journal at:
https://asmedigitalcollection.asme.org/turbomachinery

Omar Aqel[1]
Energy, Sustainability and Net-Zero Research Centre,
School of Science and Technology,
City, University of London,
London EC1V 0HB, UK
e-mail: omar.aqel@city.ac.uk

Martin White
Energy, Sustainability and Net-Zero Research Centre,
School of Science and Technology,
City, University of London,
London EC1V 0HB, UK;
Thermo-Fluid Mechanics Research Centre,
School of Engineering and Informatics,
University of Sussex, Falmer,
Brighton BN1 9RH, UK
e-mail: martin.white@sussex.ac.uk

Abdulnaser Sayma
Energy, Sustainability and Net-Zero Research Centre,
School of Science and Technology,
City, University of London,
London EC1V 0HB, UK
e-mail: a.sayma@city.ac.uk

Loss Analysis in Radial Inflow Turbines for Supercritical CO_2 Mixtures

Recent studies suggest that CO_2 mixtures can reduce the costs of concentrated solar power plants. Radial inflow turbines (RIT) are considered suitable for small to medium-sized CO_2 power plants (100 kW to 10 MW) due to aerodynamic and cost factors. This paper quantifies the impact of CO_2 doping on RIT design by comparing 1D mean-line designs and aerodynamic losses of pure CO_2 RITs with three CO_2 mixtures: titanium tetrachloride ($TiCl_4$), sulfur dioxide (SO_2), and hexafluorobenzene (C_6F_6). Results show that turbine designs share similar rotor shapes and velocity diagrams for all working fluids. However, factors like clearance-to-blade height ratio, turbine pressure ratio, and fluid viscosity cause differences in turbine efficiency. When normalized for these factors, differences in total-to-static efficiency become less than 0.1%. However, imposing rotational speed limits reveals greater differences in turbine designs and efficiencies. The imposition of rotational speed limits reduces total-to-static efficiency across all fluids, with a maximum 15% reduction in 0.1 MW CO_2 compared to a 3% reduction in $CO_2/TiCl_4$ turbines of the same power. Among the studied mixtures, $CO_2/TiCl_4$ turbines achieve the highest efficiency, followed by CO_2/C_6F_6 and CO_2/SO_2. For example, 100 kW turbines achieve total-to-static efficiencies of 80.0%, 77.4%, 78.1%, and 75.5% for $CO_2/TiCl_4$, CO_2/C_6F_6, CO_2/SO_2, and pure CO_2, respectively. In 10 MW turbines, efficiencies are 87.8%, 87.3%, 87.5%, and 87.2% in the same order. [DOI: 10.1115/1.4064193]

Keywords: radial inflow turbine, CO_2 mixtures, transcritical CO_2 cycles, turbine aerodynamic design, loss analysis

1 Introduction

Recent research has shown the advantage of CO_2 mixtures over pure CO_2 and state-of-the-art steam Rankine cycles when used in power blocks of concentrated solar power (CSP) plants. Studies under the umbrella of the SCARABEUS project have posited that mixtures of $CO_2/TiCl_4$, CO_2/SO_2, and CO_2/C_6F_6 may achieve cycle efficiencies above 50% depending on the cycle layout, turbine inlet temperature, and minimum cycle temperature; which may be as high as 60°C in the case of CO_2/SO_2 [1–4]. Most recently, it was found that mixtures outperform pure sCO_2 or steam cycles in both energy and exergy efficiencies, a difference which increases at higher ambient temperatures [5].

Another line of CO_2 mixture research is being pursued by Valencia–Chapi and co-authors. In a group of four studies, they investigated 16 mixtures for CSP power blocks. All of their studies show an increase in cycle efficiency compared to pure sCO_2. Similar to the SCARABEUS project, they found that the gains in efficiency depend on the choices of dopant, cycle layout, heat sink temperature, and mode of cooling [6–9]. Research into CO_2 mixture power blocks has also been gaining momentum with other research groups, some of which attest to the potential benefits of the technology for plants with elevated cooling temperatures [10–16]. Overall, this technology seems promising for CSP plants with relatively high heat sink temperatures (above 40°C).

According to the criteria presented by Di Marcoberardino et al. [17], the dopants for CSP applications must be able to create mixtures with critical temperatures above 85°C (0.9 of the critical temperature), and maintain thermal and chemical stability at high temperatures (700°C) and pressures (25 MPa).

Having established the latent advantages of CO_2 mixture working fluids, a component-level design study becomes justified. Owing to its relative infancy, research into CO_2 mixture turbines is limited. Although there is an existing body of literature on turbines operating with organic mixtures for organic Rankine cycles, they do not encounter the same technical challenges as those facing CO_2 turbines; namely aerodynamic and rotordynamic constraints imposed by a high-power density and high operating temperatures. Nonetheless, there have been many investigations into pure supercritical CO_2 turbines, of which only those pertaining to radial inflow turbines (RIT) are relevant to this paper.

The largest RIT thus far was investigated by El Samad et al. [18] who assessed the performance of a 100 MW utility scale RIT operating within an Allam cycle. Depending on the pressure ratio, the designed turbine may achieve total-to-static efficiencies of up to 86%, with lower pressure ratios improving efficiencies. A similar observation was made by Uusitalo and Grönman [19]. In that study, the turbine efficiency ranged between 80% and 87% for

[1]Corresponding author.

Manuscript received September 11, 2023; final manuscript received November 26, 2023; published online January 16, 2024. Tech Editor: David G. Bogard.

 Copyright © 2024 by ASME; reuse license CC-BY 4.0

Downloaded from http://asmedigitalcollection.asme.org/turbomachinery/article-pdf/146/5/051003/7230669/turbo_146_5_051003.pdf by guest on 08 March 2024

0.1 MW and 3.5 MW capacity RIT. Moreover, passage and exit losses had the greatest adverse effect on turbine efficiency.

By mapping the design space of radial turbines of different power outputs (100 kW and 200 kW), Qi et al. [20] demonstrated how recommended parameter constraints limit an RIT design space. According to that paper, total-to-static efficiencies in the range of 72–82% were possible. However, those efficiencies were likely underestimated by at least 2% because the authors of that paper had doubled the passage losses based on an erroneous implementation of the passage loss model.

There have been some studies addressing aerodynamic losses in sCO_2 RITs. Zhou et al. [21] pointed out the vulnerability of sCO_2 RIT to tip clearance due to their relatively compact size. They demonstrated this by analyzing a 1 MW RIT using computational fluid dynamics (CFD). An increase in the dimensionless tip clearance of 6% (from 2% to 8% of the leading edge height) was shown to decrease efficiency by 3.84%. They also showed that the addition of a volute may reduce efficiency by 2%.

Lv et al. [22] analyzed loss correlations using 1D generated designs and CFD simulation results. Based on their analysis, a specific set of nozzle and rotor loss models was recommended. An even more comprehensive rotor loss assessment study, including 30 different models (some of which with their own variations), was conducted by Persky and Sauret [23]. Both studies agree that the best choice of passage loss model is that developed by Wasserbauer and Glassman [24] at NASA; however, Persky and Sauret noted that the CETI model, presented by Moustapha et al. [25], is more accurate in estimating design-point efficiency. On the other hand, a study by Uusitalo and Grönman [19] concluded that the CETI model was a better option for modeling passage loss in sCO_2 turbines, specifically for specific speeds in the range of 0.4–0.65. Alternatively, Ventura et al. [26] used a combination of both approaches and averaged their results.

Thus far, many questions about the effect of doping CO_2 on the design of radial inflow turbines remain unanswered: Will the shape and dimensions of the turbine change? Will certain mixtures produce better performing turbines? What will be the similarities and differences between the mixtures? Will differences remain if the turbines operate within similar boundary conditions? And, does the scale of the turbine effect mixtures to the same degree? In this paper, these questions are answered by analyzing and comparing the design of radial inflow turbines for CO_2, $CO_2/TiCl_4$, CO_2/SO_2, and CO_2/C_6F_6 working fluids. First, RITs are designed for the four working fluids under three design scenarios at three power scales. Then, the contribution of losses in each case is reasoned and compared amongst the fluids; followed by a mathematical treatment of loss models to ascertain the effect of each of their parameters. The similarities and dissimilarities between the working fluids are then summarized based on the preceding analyses. Finally, practical rotational speed limitations are imposed to reveal its discrepant effect on the fluids. Ultimately, this study aims to better understand the consequences of doping CO_2 by explaining the root cause of the differences between radial inflow turbine designs for CO_2 mixtures.

2 Methodology

2.1 Cycle Model. A simple recuperated transcritical cycle was chosen for the purpose of this study. A schematic of the cycle and its temperature–entropy (T–s) diagram are shown in Fig. 1. Turbine boundary conditions, including dopant fraction, are derived from an optimization study conducted by the authors in a previous study [27]; the results of which are shown in Table 1.

2.2 Turbine Model. Conventionally, radial inflow turbines are designed by assuming a set of geometric and kinematic parameters, the values of which are based on recommendations from the literature. At first, the rotor geometry and kinematics are defined, which in turn inform the nozzle and volute designs. Most literature follow one of the three most popular design methodologies introduced by: (1) Aungier [28]; (2) Moustapha et. al. [25]; and (3) Whitfield [29]. Lee and Gurgenci [30] compared the three against experimental data and studied their consequences on rotor design. All three methods yield turbine efficiencies within 2% of each other, with the latter method resulting in the lowest efficiency due to faster flow velocities.

In this study, the flow coefficient (ϕ), the loading coefficient (ψ), and the meridional velocity ratio (ζ) are used to determine the velocity triangles, following the method suggested by Mustapha et al. [25]. They are defined as

$$\phi = \frac{C_{5m}}{U_4} \tag{1}$$

$$\psi = \frac{\Delta h_0}{U_4^2} \tag{2}$$

$$\zeta = \frac{C_{5m}}{C_{4m}} \tag{3}$$

where Δh_0 (J/kg) is the total-to-total enthalpy drop across the turbine, and the velocities U_4, C_{4m}, and C_{5m} are indicated in Fig. 2. Additionally, the hub-to-shroud (r_{5h}/r_{5sh}) and the outlet-to-inlet (r_5/r_4) radius ratios are used to control the turbine shape. In Fig. 3, key dimensions of the turbine rotor are shown, whereas the velocity triangles and labeling convention of the tangential and meridional directions are shown in Fig. 2.

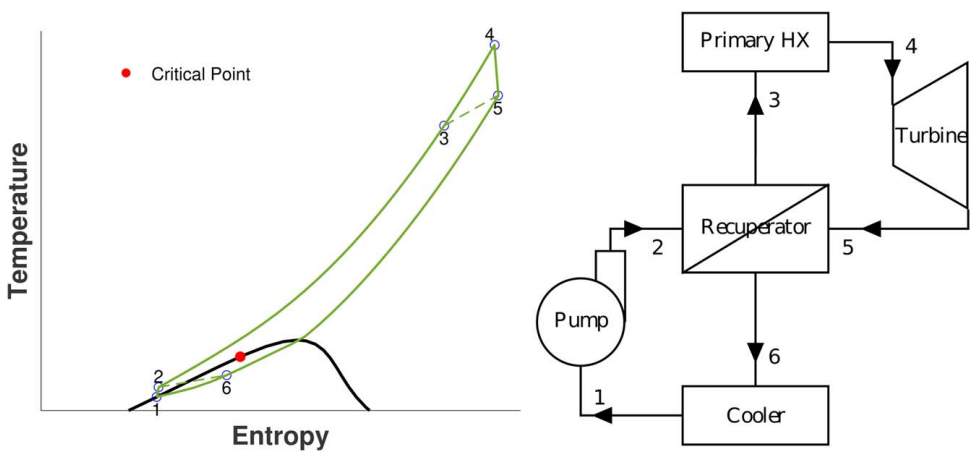

Fig. 1 T–s diagram and schematic of a simple recuperated tCO_2 cycle

Downloaded from http://asmedigitalcollection.asme.org/turbomachinery/article-pdf/146/5/051003/7230669/turbo_146_5_051003.pdf by guest on 08 March 2024

Table 1 Turbine boundary conditions

Variable	$CO_2/TiCl_4$	CO_2/SO_2	CO_2/C_6F_6	CO_2
Additive (%)	17	26	17	0
T_{in} (°C)	700	700	700	700
P_{in} (MPa)	25	25	25	25
$P_{in,t}/P_{out,s}$	2.50	3.39	3.25	3.42

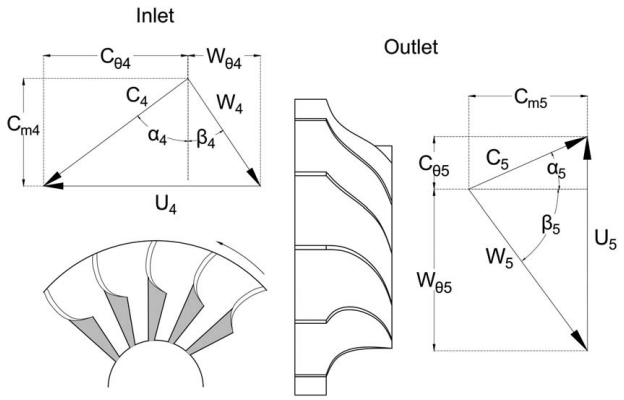

Fig. 2 Radial inflow turbine velocity diagrams

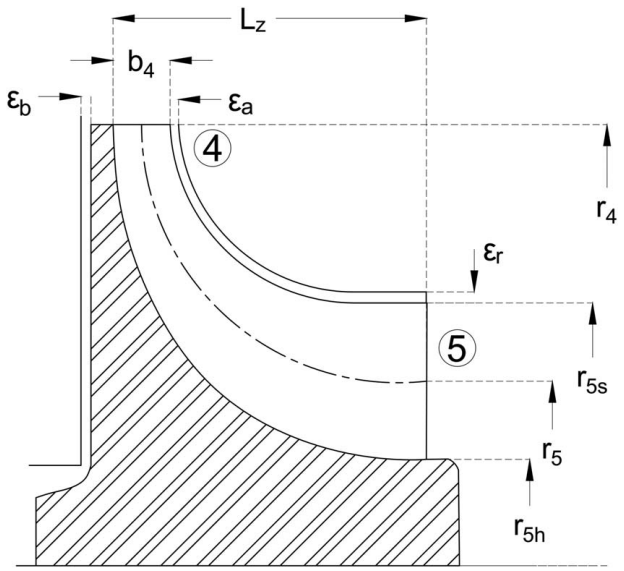

Fig. 3 Radial inflow turbine meridional geometry

The turbine design and performance evaluation process is initiated by specifying the turbine boundary conditions, design variables, and fixed parameters which are then used to generate the rotor geometry and flow kinematics. Subsequently, aerodynamic losses are computed using a set of loss models. Table 2 lists the loss mechanisms considered, along with an abbreviation of the correlations chosen to represent each of the losses, and a reference to the source where the complete forms of the correlations can be found.

The nozzle loss was chosen because it relates the loss to geometry and flow parameters. The passage and clearance losses, which typically comprise more than 60% of the total loss, were chosen based on their accuracy in predicting design-point efficiency [23]. The same study recommends the incidence and trailing edge losses in Eqs. (9) and (12). The choice of windage loss is less consequential as it contributes little to the total loss in efficiency.

The total enthalpy loss in the turbine is equal to the arithmetic sum of individual aerodynamic losses

$$\Delta h_{\text{loss}} = \Delta h_{\text{n}} + \overbrace{\Delta h_{\text{i}} + \Delta h_{\text{p}} + \Delta h_{\text{c}} + \Delta h_{\text{te}}}^{\Delta h_{\text{rotor}}} + \Delta h_{\text{e}} \tag{4}$$

Total-to-static and total-to-total efficiencies are calculated as

$$\eta_{\text{ts}} = \frac{h_4 - h_5}{h_4 - h_{5\text{s}}} \tag{5}$$

$$\eta_{\text{tt}} = \frac{h_4 - h_5}{h_4 - h_{05\text{s}}} \tag{6}$$

Unlike other losses, the enthalpy drop due to windage is subtracted from the total enthalpy drop when calculating the power

$$W = \dot{m}(\Delta h_{\text{tt}} - \Delta h_{\text{w}}) \tag{7}$$

Therefore, it is not considered as an internal loss in the rotor and does not contribute to the entropy generation between the rotor inlet and outlet.

2.3 Model Verification and Validation. The process of verification aims to confirm the sanctity of the 1D mean-line model by demonstrating that it generates results consistent with other 1D mean-line models. This may be achieved by simulating existing 1D turbine designs and comparing the results with that of the source. Model verification is made complicated because it is uncommon to find existing works which use an identical mean-line design approach to the one used here. Alternatively, a sensible approach to verification is to tailor the mean-line model to match the assumptions of the existing models whilst maintaining core features intact.

Validation, on the other hand, proves the accuracy of the 1D model, not its consistency. Validation is necessary because the loss equations used in the mean-line design model were originally created for air turbines. Therefore, it is imperative to confirm their accuracy in the design of non-air gas turbines before interpreting the results of the mean-line model. Ideally, the mean-line model results would be benchmarked against experimental data points. However, in the absence of experimental data, a numerical model, such as CFD, is commonly used in lieu of experiments. Fortunately, LV et al. [22] validated their mean-line model with CFD simulations. Therefore, verification of the current 1D model against that study would validate it by corollary. To ensure a fair comparison, the 1D mean-line model was temporarily modified to neglect blade blockage at both the leading and trailing edges of the rotor, as was the case in the source study [22].

Two versions of the 1D model are compared in Table 3: one that neglects blade blockage in accordance with the source study; the other accounts for blockage. The former is a temporary modification to the model which is used exclusively for comparison, but is discarded otherwise.

With the regards to the modified model, although blockage is not accounted for, there are differences in most parameters, the greatest of which is in the leading edge height b_4 with a deviation of −11% from the source. This is because the modified model produces a greater inlet radius r_4, which is a consequence of the greater tip speed U_4. The higher tip speeds are attributed to the overestimation of the inlet velocity C_4. Ultimately, all these differences originate from the enthalpy loss through the stator; the model estimates lower loss compared to Ref. [22].

The same may be inferred with respect to the current model which accounts for blade blockage, as listed in the last column of Table 3. However, the differences in the geometric parameters are greater because the passage is partly blocked by the blades, thus larger radii are required to maintain the same passage areas.

Overall, the discrepancies culminate in an efficiency difference of ~1%. A loss breakdown of the current turbine design and that as

Downloaded from http://asmedigitalcollection.asme.org/turbomachinery/article-pdf/146/5/051003/7230669/turbo_146_5_051003.pdf by guest on 08 March 2024

Table 2 Loss equations used in the 1D mean-line model

Loss mechanism	Correlation	Equations	References
Nozzle	$\Delta h_{\mathrm{n}} = \frac{C_4^2}{2}\frac{0.05}{Re_{\mathrm{N}}^{0.2}}\left(\frac{3\tan\alpha_4}{s/c} + \frac{s\cos\alpha_4}{b_4}\right)$	(8)	[37]
Incidence	$\Delta h_{\mathrm{i}} = \frac{W_4^2}{2}(\sin(\beta_4 - \beta_{4,\mathrm{opt}}))^2$	(9)	[24]
Passage	$\Delta h_{\mathrm{p}} = m_{\mathrm{f}}\left[\frac{L_{\mathrm{h}}}{D_{\mathrm{h}}} + 0.68\left(1 - \left(\frac{r_5}{r_4}\right)^2\right)\frac{\cos\beta_5}{b_5/c}\right]\frac{W_4^2 + W_5^2}{2}$	(10)	[25]
Clearance	$\Delta h_{\mathrm{c}} = \frac{Z_{\mathrm{r}}U_4^3}{8\pi}(K_{\mathrm{a}}\varepsilon_{\mathrm{a}}C_{\mathrm{a}} + K_{\mathrm{r}}\varepsilon_{\mathrm{r}}C_{\mathrm{r}} + K_{\mathrm{ar}}\sqrt{\varepsilon_a\varepsilon_{\mathrm{r}}C_{\mathrm{a}}C_{\mathrm{r}}})$	(11)	[25]
Trailing edge	$\Delta h_{\mathrm{te}} = \left(\frac{Z_{\mathrm{r}}t_5}{\pi(r_{5\mathrm{s}} + r_{5\mathrm{h}})\cos\beta_5}\right)\frac{W_5^2 Y_5}{2}$	(12)	[38]
Exit	$\Delta h_{\mathrm{e}} = \frac{C_5^2}{2}$	(13)	
Windage	$\Delta h_{\mathrm{w}} = 0.25C_{\mathrm{w}}\rho_4\omega^2 r_4^5$	(14)	[39]

Table 3 Mean-line model verification against Ref. [22]

Input	Ref. [22]	$\mathrm{Model}_{\mathrm{noblockage}}$		Model	
$\dot{m}$ (kg/s)	1.80	1.80		1.80	
T_{04} (K)	943	943		943	
p_{04} (bar)	106.9	106.9		106.9	
p_6 (bar)	77.7	77.7		77.7	
N (krpm)	80.0	80.0		80.0	
Z_r	14.0	14.0		14.0	
Z_n	21.0	21.0		21.0	
ε (mm)	0.30	0.30		0.30	
t_4 (mm)	0	0		1.24	
t_{5s} (mm)	0	0		0.31	
t_{5h} (mm)	0	0		0.62	
ϕ	0.88	0.88		0.88	
ψ	0.28	0.28		0.28	
ξ	1.14	1.14		1.14	
r_5/r_4	0.48	0.48		0.48	
r_{5h}/r_{5s}	0.50	0.50		0.50	
α_4 (deg)	76.5	76.5		76.5	
Results		dev (%)		dev (%)	
r_4 (mm)	27.3	27.8	2	31.0	14
r_{5s} (mm)	17.5	16.9	−3	18.9	8
r_{5h} (mm)	8.69	8.38	−4	9.36	8
b_4 (mm)	4.48	3.99	−11	3.93	−12
β_4 (deg)	28.5	−29.6	4	−29.6	4
$\beta_{5,rms}$ (deg)	58.7	−63.4	8	−63.4	8
U_4 (m/s)	228	233	2	232	2
C_4 (m/s)	208	211	1	210	1
W_4 (m/s)	55.6	56.5	2	56.5	2
C_6 (m/s)	55.3	56.0	1	55.9	1
W_6 (m/s)	123	125	2	125	2
η_{ts} (%)	83.1	84.2	1.1	84.0	0.9
η_{tt} (%)	85.4	86.6	1.2	86.4	1

reported by Ref. [22] is shown in Fig. 4. The loss profiles are well aligned apart from small differences in the passage and clearance losses, which are likely due to the deviations in velocities. The greatest difference is in the stator loss. This is expected because the source study uses a different stator loss model that only depends on the flow velocity and a loss coefficient, unlike the model used here in Eq. (8), which also accounts for the angle of the flow and the viscosity of the fluid.

The mean-line model is further validated for all the working fluids using CFD for one of the design cases discussed in Sec. 3, namely the 1 MW turbine of case A with the rotational speed limit imposed. A comparison of key variables of the mean-line and CFD simulations are listed in Table 4.

The 3D geometry of the rotor blade was built in ANSYS BLADEGEN using the blade inlet and outlet geometries generated by the mean-line model. The stator was designed according to the method detailed by Ref. [28], then built in SOLIDWORKS and imported into ANSYS DESIGNMODELER. The 3D rotor and stator blades and their passages were meshed using ANSYS TURBOGRID. The mesh resolution was determined from mesh-dependence study for both the rotor and stator, the results of which are shown in Fig. 5. The final mesh was composed of approximately 770,000 nodes in the rotor, and 460,000 nodes in the stator.

Simulations were then conducted using ANSYS solver. The Reynolds-averaged Navier–Stokes equations were closed with the $k-\varepsilon$ turbulence model. Boundary conditions were imposed as total conditions at the inlet and static pressure at the exit of the domain. Solution convergence was achieved if the root mean square residuals for mass, momentum, and turbulence had reduced to at least 10^{-5}. Thermodynamic and transport properties were supplied to the CFD solver by a lookup table created with properties calculated by SIMULINK THERMODYNAMICS software package. The size of the lookup table was 200×200 and spans the range of $7<P<30$ MPa and $700<T<950$ K. The table resolution was determined based on a sensitivity study; the results of which indicated that increasing the resolution beyond 200 would have an insignificant effect on the efficiency or mass flow (less than 0.01%).

2.4 Turbine Design Optimization. In the following study, radial inflow turbines are designed for four working fluids under three scenarios and three power capacities. In all instances, the turbines are assumed to operate under similar inlet conditions, namely

Downloaded from http://asmedigitalcollection.asme.org/turbomachinery/article-pdf/146/5/051003/7230669/turbo_146_5_051003.pdf by guest on 08 March 2024

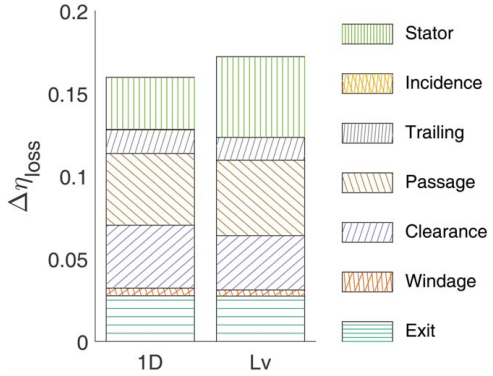

Fig. 4 Loss comparison with Ref. [22]

Table 4 Mean-line model verification against CFD

Fluid	Variable	Model	CFD	dev (%)
$CO_2/TiCl_4$	η_{tt} (%)	88.94	91.57	−2.63
	η_{ts} (%)	87.02	86.88	0.14
	$\dot{m}$ (kg/s)	23.98	24.13	−0.63
	Power (MW)	10.003	10.086	−0.82
CO_2/SO_2	η_{tt} (%)	88.91	90.79	−1.88
	η_{ts} (%)	86.95	85.95	1.00
	$\dot{m}$ (kg/s)	17.14	17.40	−1.50
	Power (MW)	10.003	10.008	0.05
CO_2/C_6F_6	η_{tt} (%)	88.87	91.55	−2.68
	η_{ts} (%)	87.12	85.66	0.16
	$\dot{m}$ (kg/s)	22.82	22.96	−0.62
	Power (MW)	10.007	10.006	−0.54
CO_2	η_{tt} (%)	88.23	91.44	−2.68
	η_{ts} (%)	85.66	85.57	0.1
	$\dot{m}$ (kg/s)	15.32	15.65	−2.13
	Power (MW)	10.0	10.2	2.08

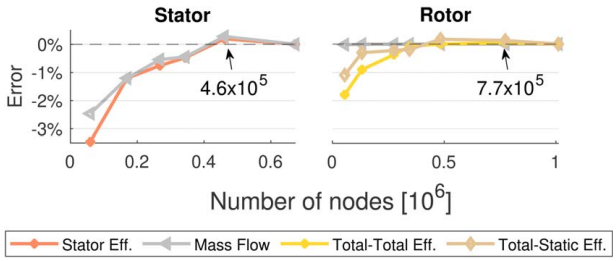

Fig. 5 Grid independence study for rotor and stator

total temperature and pressure; but, the static outlet pressure and mass flowrate depend on the scenario and the power capacity, respectively.

In cases B and C, a gradient-method optimization algorithm is used with Eq. (5) as the objective function; hence the turbines are optimized to maximize the total-to-static efficiency. Moreover, a global optimum solution is ensured by initiating the optimizer ten times, each time from a randomly chosen initial point. The number of initiation points was determined by a sensitivity study through which the optimal solution remained unchanged above five initiation points; twice that number was used for the sake of certainty.

2.4.1 Case A: Fixed Design and Pressure Ratio. In the first instance, all design parameters are selected and fixed based on common recommendations in the literature, which are listed in Table 6. This exercise aims to study the effectiveness of the standard approach in choosing an efficient design for each of the working fluids. Moreover, the pressure ratio is also fixed according to the cycle conditions under which each working fluid is designed to operate, as listed in Table 1. Although these pressure ratios may not maximize turbine performance, they are the typical conditions under which the turbines are expected to operate.

2.4.2 Case B: Optimized Design at Fixed Pressure Ratio. Next, the pressure ratios are maintained according to the cycle, but the input design parameters are optimized within the constraints shown in Table 6. The range of each of these parameters that yields good turbine performance is well-established in the literature and will be used to confine the turbine design space. This iteration represents a thorougher design approach than case A because more effort is required to find the optimal design rather than relying on a one-size-fits all approach.

2.4.3 Case C: Optimized Design and Pressure Ratio. Finally, the pressure ratios are optimized along with the input parameters of case B. The change in pressure ratio is balanced by a change in mass flowrate to maintain a prescribed power output. This scenario decouples the turbine pressure ratio from that of the cycle pressure ratio. This exercise aims to determine whether the turbines will converge on a common pressure ratio, whether the differences between the fluids are caused by the turbine boundary conditions rather than intrinsic differences between the fluids themselves, and it will also indicate the potential benefit of multi-staging in each of the working fluids.

2.4.4 Power Scaling. Large scale designs may suppress the differences among the working fluids. Therefore, the three aforementioned cases are simulated for turbines with power outputs of 0.1 MW, 1 MW, and 10 MW. Ultimately, power scaling will reveal whether certain mixtures have an inherent advantage at smaller scales.

3 Results and Discussion

This section explores turbine designs for pure and mixed CO_2 working fluids under the three design approaches across power scales. First, the performance of all the cases is discussed in terms of total-to-static efficiency. Second, the loss breakdown of case B against case C is presented to explain the observed trends. Next, particular interest is given to clearance loss owing to its importance at smaller scales. Lastly, similarities and dissimilarities between the fluids are highlighted.

3.1 Performance Trends. The following discussion refers to the total-to-static efficiencies presented in Fig. 6.

3.1.1 Power Scaling. Regardless of the working fluid, the gain in efficiency from 0.1 MW to 1 MW is always greater than the gain from 1 MW to 10 MW. Apart from a few cases, the former is more than double the latter. Among the fluids, the increase in efficiency with power scaling is greatest for CO_2, regardless of the design approach (case A, B, or C). At its greatest, the gain in efficiency is 12% between 0.1 MW and 10 MW for case A of CO_2. The smallest gains are ~5.4% between 0.1 MW and 10 MW for case C of $CO_2/TiCl_4$ and CO_2/C_6F_6.

The power a turbine generates scales with the radius squared, but the leakage flow scales linearly with the radius [31]. Therefore, avoiding leakage losses is easier in large turbines, but will be difficult in small-scale turbines. Ultimately, the clearance gap-to-blade height ratio is the best indicator of the loss in efficiency due to leakage.

The consequence of the clearance-to-blade height ratio is best understood through Fig. 7, in which designs according to case A are presented. Case A was chosen because the discrepancies between the fluids are most pronounced, whereas the differences are lessened by the optimization in cases B and C. There is a

Downloaded from http://asmedigitalcollection.asme.org/turbomachinery/article-pdf/146/5/051003/7230669/turbo_146_5_051003.pdf by guest on 08 March 2024

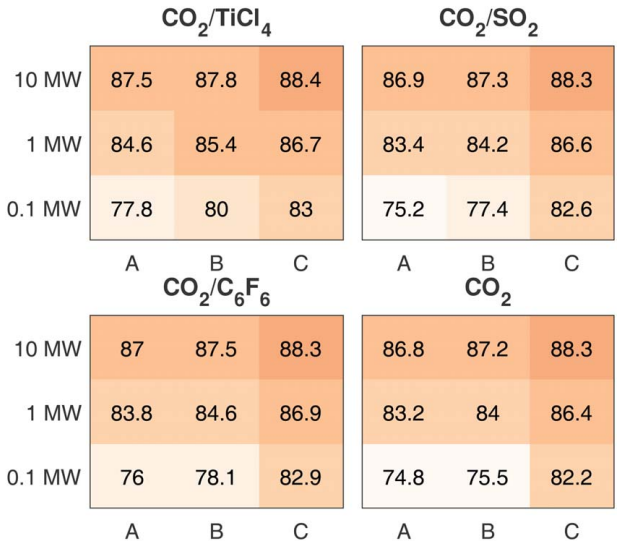

Fig. 6 Total-to-static efficiency of the three cases at different power capacities

direct but inverse correlation between the total-to-static efficiency and the clearance-to-height ratio; the greater the ratio, the lower the efficiency. Because $CO_2/TiCl_4$ can maintain the lowest ε/b_4 across scales, it has the highest turbine efficiency amongst the fluids, which is confirmed by Fig. 6. Conversely, CO_2 has the greatest (ε/b_4), thus the lowest efficiency.

Although the trends in efficiency and ε/b_4 are observably correlated, they do not necessarily prove causation. However, causation is demonstrated in the same figure by the parallel lines of efficiency at the top of the figure. These lines were produced by running similar scenarios as in case A; but with a constant clearance-to-blade height ratio $\varepsilon/b_4 = 0.02$. This assumption is for illustrative purposes and may not be feasible as the clearance gap may be as low as 22 μm in 0.1 MW turbines. Although narrower gaps have been cited in the literature [20], their feasibility was not physically demonstrated.

This hypothetical example demonstrates that if ε/b_4 is assumed constant, the change in efficiency across scales becomes uniform for all fluids, thus negating the positive effect wider blade heights have on efficiency. It also indicates the potentially significant gain in efficiency if shrouded rotors are used, especially at small scale. Of course, the use of shrouds will be accompanied by greater windage loss; nonetheless, the potential gains due to the reduction in clearance loss will likely outweigh the penalties of windage loss. The factors limiting the use of closed rotors are likely to be mechanical. First, the structural limits placed on the blade tip speeds are more stringent when closed shrouds are used. Generally, tip speeds should be lower with closed rotors. Moreover, the manufacturability of the closed rotor passages at such small scales is a key hindrance, as well as the increased mass and the effect this might have on rotordynamics—particularly at the smaller scales.

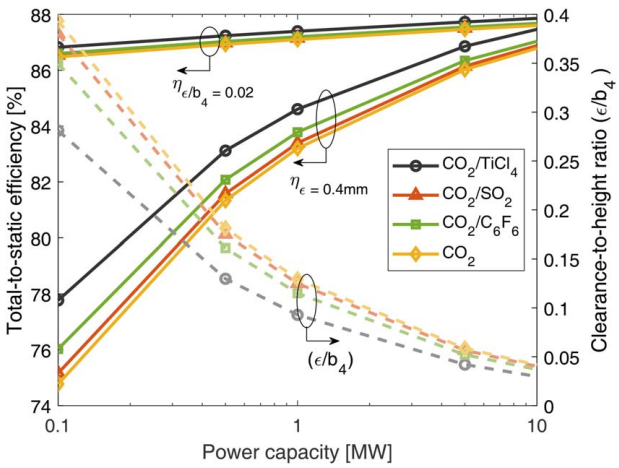

Fig. 7 Left axis: change in efficiency across power scales at constant $\varepsilon = 0.4$ mm, and at constant clearance-to-height ratio $\varepsilon/b_4 = 0.02$; right axis: the change in ε/b_4 when $\varepsilon = 0.4$ mm

The larger blade heights in $CO_2/TiCl_4$ turbines is a consequence of the lower specific work of the turbine, which causes higher mass flowrates to maintain the same power output. Evidently, this is due to the difference in the inlet density of the fluid and, to a lesser degree, its adiabatic coefficient, as explained in an earlier publication [32]. Although the difference in the blade heights is exacerbated by the difference in the pressure ratio between the working fluids, it is not eliminated even if a uniform pressure ratio is applied to all fluids, as is discussed in the following section.

3.1.2 Design Scenarios. The merits of design optimization are evident in all fluids and for all power capacities. As stated earlier, case A assumes both fixed design parameters and pressure ratios, whereas case B optimizes the design variables but maintains the same pressure ratios. Therefore, any differences between the two approaches will be a result of the change in turbine design parameters. Overall, case B improves the performance of all turbines, indicating that optimization converges on design parameters that are more suitable than those assumed in case A.

A greater gain in the efficiency of case B indicates a greater inadequacy of the assumptions of case A. This is most apparent at small scales where the differences between the two cases are the greatest. Therefore, small turbines require a different set of design parameters than those assumed in case A. For example, the smallest gain in design parameter optimization is 0.3% for 10 MW $CO_2/TiCl_4$, and the greatest is 2.2% for 0.1 MW CO_2/SO_2. For all fluids, as the turbines are scaled up toward 10 MW, the differences between case A and case B decrease, thus indicating that the assumption of case A is better suited to 10 MW turbines.

The turbine is decoupled from cycle conditions in case C by optimizing the static pressure at the outlet, thus the turbine pressure ratio is optimized. Case C also optimizes design parameters. Therefore, performances differences between case C and case B are derived from pressure ratio optimization even if the design parameters are different.

For all working fluids, the optimization algorithm converges on the minimum limit of the pressure ratio (1.5) by maximizing the outlet pressure. This is an expected outcome because lower pressure ratios induce lower flow velocities and, consequently, lower aerodynamic losses; which is true across power capacities. Here, as in case B, small turbines benefit the most from pressure ratio optimization. The greatest increase in efficiency for case C compared to case B is 6.7% with 0.1 MW CO_2 turbine, and the smallest increase is 0.6% with 10 MW CO_2.

Among the fluids, the smallest gain in pressure ratio optimization is for $CO_2/TiCl_4$. This is because the pressure ratio set by cycle conditions, as used for cases A and B, is lower than those of the other fluids, as listed in Table 1. Therefore, the change in the pressure ratio for $CO_2/TiCl_4$ is 1.0 compared to 1.75, 1.89, and 1.92 for CO_2/SO_2, CO_2/C_6F_6, and CO_2, respectively. This suggests that $CO_2/TiCl_4$ will benefit less from multi-staging compared to the other fluids when operating within pressure ratios dictated by their respective cycles.

Generally, the benefits of scaling are greater for case A, followed by case B and the case C, regardless of the working fluid. Therefore, the differences in the efficiencies of the cases for a given power capacity decrease at higher power scales. For example, the efficiency of case C is 7.4% higher than that of case A for 0.1 MW CO_2/SO_2, but this difference shrinks to 1.4% at a scale of 10 MW. A similar trend is observed in all fluids, but to varying degrees. The cause of the dissimilar trends in performance across

Downloaded from http://asmedigitalcollection.asme.org/turbomachinery/article-pdf/146/5/051003/7230669/turbo_146_5_051003.pdf by guest on 08 March 2024

power scales is the drastic change in the height of the clearance gap at the blade with respect to the height of the blade, as was explained through Fig. 7.

An apt comparison of fluids, cases, and power scales may be made through a classical specific speed and efficiency chart. In Fig. 8, all turbines discussed thus far are plotted with respect to the curve produced by Balje [33]. The benefits of optimization are evident in case B and case C where the efficiency is higher than case A, especially in 0.1 MW turbines. Moreover, the higher flow coefficients result in higher specific speeds in cases B and C. Overall, designs fall in the range of $0.3 < N_s < 0.5$;.

3.2 Loss Analysis. The loss profiles of the optimal RIT designs according to case B are presented in Fig. 9. Overall, the contributions of losses are similar for all fluids, with the rotor passage loss having the greatest weight in 10 MW turbines, clearance and passage equally contributing to losses in 1 MW turbines, and clearance as the predominate loss in 0.1 MW turbines. Among all losses, however, the clearance loss is the most salient variance across power scales. In the proceeding analysis, the similarities across the working fluids are explained, followed by a discussion on the variance across power scales.

Stator and exit losses mainly depend on the absolute inlet and outlet velocities, respectively. Therefore, the stator and exit losses are almost uniform among the fluids at the same power scale owing to the similar velocity diagrams at inlet and outlet, an example of which is shown in Fig. 10. The sizes of the triangles scale with the specific work of the turbine, but the shapes are determined by ψ, ϕ, and ζ. Although stator loss is also dependent on the kinematic viscosity of the working fluid, as shown in Eq. (8), it will be shown in Sec. 3.3 that this dependency is weak.

Across power scales, however, there is an increase in the stator loss and a more notable increase in the exit loss. Velocity diagrams may also be used to explain these increases. An example is shown in Fig. 11 for CO_2/SO_2, in which the outlet velocity is greater in small turbines, which is driven by the increase in the flow coefficient (ϕ).

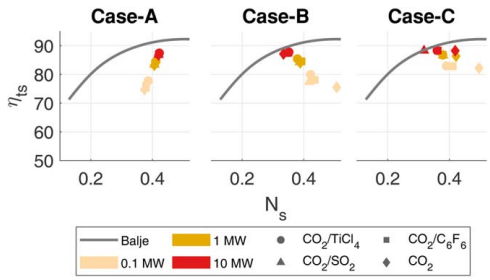

Fig. 8 Specific speed and efficiency comparison

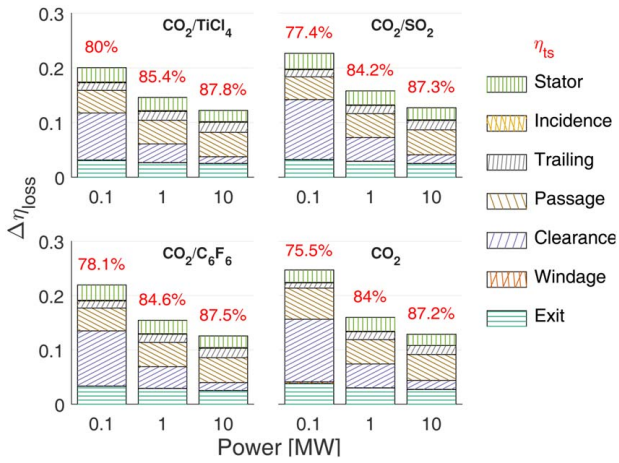

Fig. 9 Loss contributions for case B

This trend is observed in all working fluids and is the response of the optimization algorithm to the increasing clearance. According to the clearance loss model in Eq. (11), losses will decrease with increasing meridional velocities C_{4m} and C_{5m}. Therefore, as the significance of clearance loss amplifies at smaller scales, optimization favors designs that have higher flow coefficients. This is an attempt to abate the increase in clearance loss because of its increasing importance at small scale; which is not prevalent in larger turbines where the increase in the passage loss due to higher flow velocities outweighs the decrease in clearance loss, thus lower flow coefficients are preferred. Moreover, the inlet radius reduces in order to reduce the clearance/blade height, which would further increase the rotational speed at small scale; this is evident in the increase in the blade width to radius ratio (b_4/r_4) shown in Table 5.

Like the exit loss, the trailing edge loss is also influenced by the velocity triangle at the outlet, namely by w_5 and β_5, and to a lesser degree, by the outlet blade dimensions and the blade count. Therefore, the similar outlet velocity triangles and proximate blade counts render the trailing edge loss contributions comparable for all fluids at the same power scale. Unlike clearance loss, the trailing edge loss is less important in small turbines compared to large turbines owing to the decrease in the relative velocity at outlet w_5 and the decrease in the blade count in some fluids like $CO_2/TiCl_4$ and CO_2. Both incidence and windage losses are negligible for all fluids. The former is suppressed by the constraint of $-40 < \beta_4 < -20$ imposed

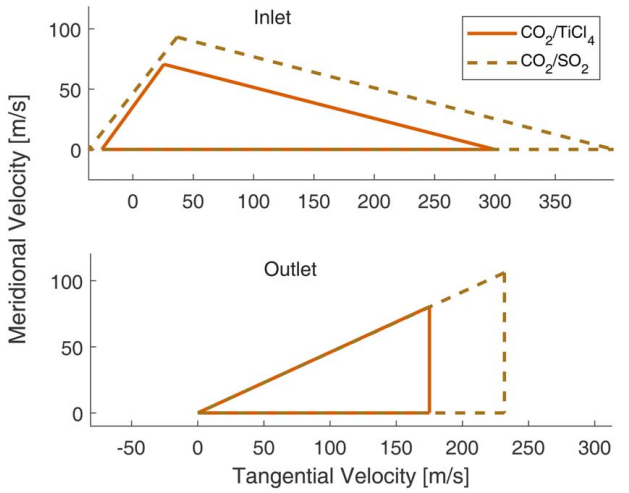

Fig. 10 Velocity triangles for 0.1 MW $CO_2/TiCl_4$ and CO_2/SO_2 turbines from case B

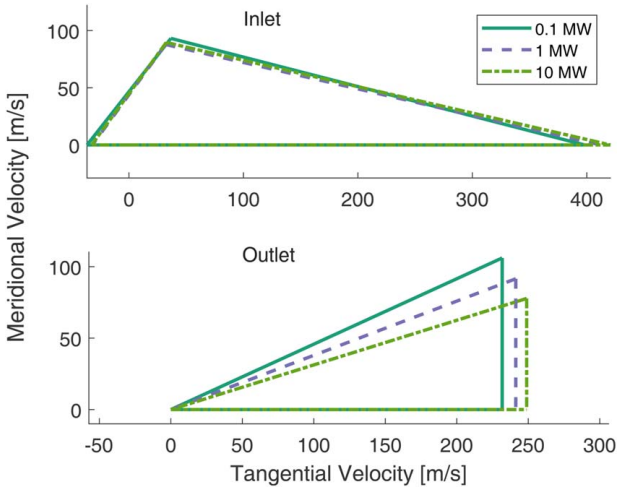

Fig. 11 Velocity triangles across power scales for CO_2/SO_2 from case B

Downloaded from http://asmedigitalcollection.asme.org/turbomachinery/article-pdf/146/5/051003/7230669/turbo_146_5_051003.pdf by guest on 08 March 2024

Table 5 Design data for optimal case B RIT

	0.1 MW				10 MW			
Parameter	$CO_2/TiCl_4$	CO_2/SO_2	CO_2/C_6F_6	CO_2	$CO_2/TiCl_4$	CO_2/SO_2	CO_2/C_6F_6	CO_2
ψ	0.9	0.91	0.91	0.88	0.92	0.92	0.92	0.86
ϕ	0.26	0.27	0.28	0.3	0.23	0.23	0.23	0.23
ξ	1	1.17	1.18	1	1	1	1	1.04
r_5/r_4	0.6	0.58	0.58	0.47	0.6	0.6	0.6	0.59
r_h/r_s	0.69	0.62	0.62	0.32	0.67	0.68	0.68	0.67
N_s	0.4	0.42	0.43	0.49	0.39	0.38	0.38	0.41
b_4/r_4 (%)	8.0	9.1	9.2	9.0	8.1	6.8	6.7	6.9
η_{tt} (%)	80	77.4	78.1	75.5	87.8	87.3	87.5	87.2
η_{ts} (%)	82.6	79.9	80.7	78.6	90.1	89.5	89.7	89.6
p_{06}/p_5	2.5	3.39	3.25	3.42	2.5	3.39	3.25	3.42
Δh_{tt} (kJ/kg)	103	186	138	212	103	186	138	212
N (krpm)	192.7	314.1	252.7	396.3	20	30.6	24.2	35.8
α_4 (deg)	73.7	75.6	75.6	71.2	76	76	76	75.6
β_4 (deg)	−20	−20.3	−20.8	−22.6	−20	−20	−20	−31.3
β_5 (deg)	−66.2	−64.8	−64.6	−57.6	−69	−69.1	−69.1	−68.8
U (m/s)	302	397	344	427	314	421	363	462

on the optimization, which maintains favorable flow angles into the rotor and keeps the loading coefficient ψ close to 0.9.

Instead of presenting an additional loss profile chart for case C, Fig. 12 shows the difference in each loss contribution with respect to the baseline case B. Compared to case B, both passage and clearance losses are lower in case C for all turbines across all power scales, while trailing edge losses are higher. This is because the lower pressure ratios of case C compared to case B require turbines that are less loaded. According to Euler's equation, the specific work of a turbine with zero exit swirl ($\alpha_5 = 0$) is defined as

$$w = U_4 C_{4\theta} \tag{15}$$

Therefore, to decrease the specific work ("unload" the turbine), the blade tip speed and or the inlet tangential velocity must be decreased. In case C, both U_4 and $C_{4\theta}$ reduce in concert to maintain a favorable absolute inlet flow angle within the limits of Table 6.

Concurrently, to maintain the prescribed power capacity at a lower specific work, the mass flowrate must increase. With slower flows and greater flowrates, the passage areas must enlarge, leading to wider blades. Ultimately, the wider blades lower clearance losses by decreasing the clearance gap-to-blade height ratio ε/b_4 in both the axial and radial directions at the inducer and exducer, respectively. Moreover, slower internal flows in the rotor decrease friction and its associated passage loss.

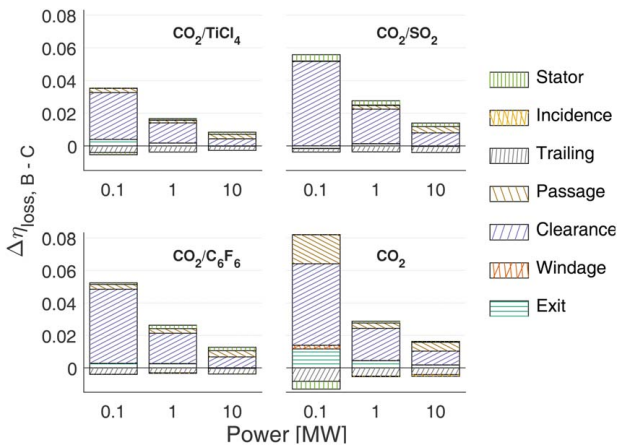

Fig. 12 Difference in loss contributions between case B and case C

On the other hand, the wider blades at the outlet induce higher trailing edge losses, as observed for all turbines.

3.3 Loss Model Sensitivity. The purpose of the following analysis is to examine and explain the sensitivity of the loss models to changes in the geometric and kinematic features of the RIT, and in the viscosity of the fluid. The ranges of the input variables are set based on the expected turbine design space, and are shown in Table 7, in which the limits of some parameters are set as a fraction of the base value, while the limits for others are set in absolute value. The base values are taken from 0.1 MW and 10 MW CO_2 turbines from case B as examples. Moreover, the exit loss is not considered in the analysis because of its direct and quadratic correlation with C_5, which will cause C_5 to overwhelm all other parameters in Fig. 13.

This analysis is purely mathematical and assumes that all terms are mutually exclusive, and thus can be changed independently of each other; which is not physically possible. However, loss models are ultimately mathematical formulas and will be treated as such for the purposes of this analysis. By understanding the effect each term has on turbine losses the optimal turbines designs presented in the preceding sections may be justified.

In Fig. 13, the qualitative significance of a parameter is indicated by the length of its bars, the bars on the left-hand side are for kinematic parameters, the bars on the right-hand side of the graph are geometric parameters, except for ν_4 which is a physical parameter, and the contrast of the color indicates the power scale: dark for 10 MW; light for 0.1 MW.

Table 6 Turbine optimization parameters

Variable	Type	Case A	Cases B and C	References
ϕ	Variable	0.23	0.2 – 0.3	[25]
ψ	Variable	0.93	0.85 – 1.0	[25]
ξ	Variable	1.0	1.0 – 1.5	[40]
r_5/r_4	Variable	0.5	0.3 – 0.7	[37,41]
r_{5h}/r_{5sh}	Variable	0.45	0.4 – 0.7	[41]
α_4 (deg)	Constraint	—	68 – 76	[42]
β_4 (deg)	Constraint	—	−20 to 40	[25]
r_{5sh}/r_4	Constraint	—	<0.7	[37]
α_5 (deg)	Input	0	0	[25]
$\varepsilon_{a,r}$ (mm)	Input	0.4	0.4	[37]
L_z/b_5	Input	1.50	1.50	[28]
t_4/r_4	Input	0.04	0.04	[40]
t_{5h}/r_4	Input	0.02	0.02	[40]
t_{5sh}/r_4	Input	0.01	0.01	[40]

Downloaded from http://asmedigitalcollection.asme.org/turbomachinery/article-pdf/146/5/051003/7230669/turbo_146_5_051003.pdf by guest on 08 March 2024

Table 7 Range of parameters for loss sensitivity study

	Fractional limits			Absolute limits		
	Lower	Upper		Lower	Upper	Unit
b_4	0.75	1.25	W_4	50	250	(m/s)
r_{5s}	0.75	1.25	W_5	50	250	(m/s)
r_{5h}	0.75	1.25	C_4	150	450	(m/s)
r_4	0.75	1.25	C_{4m}	50	250	(m/s)
L_z	0.75	1.25	C_5	50	150	(m/s)
ε	0.5	1.5	Z_r	12	32	—
ν_4	0.5	1.5	α_4	40	80	(deg)
			β_4	−40	40	(deg)
			β_5	−85	−45	(deg)

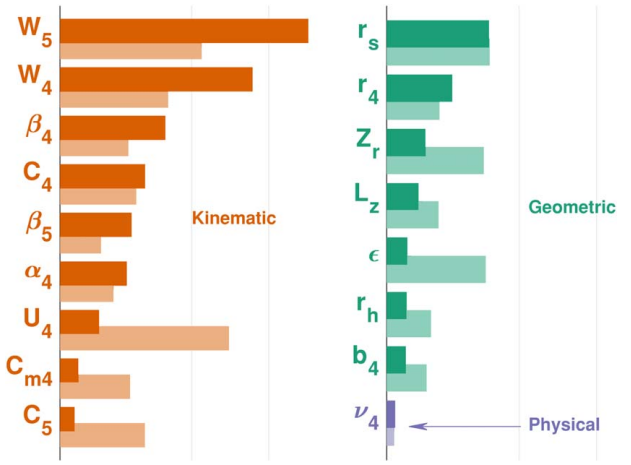

Fig. 13 Loss sensitivity: the length of the bars indicates the qualitative effect a parameter has on the total loss. The bars on the left-hand side are for kinematic parameters, the bars on the right-hand side of the graph are geometric parameters, except for ν_4 which is a physical parameter. Dark bars are for 10 MW; Light for 0.1 MW.

A perceptible feature of Fig. 13 is the uneven influence of parameters, which is dependent on the significance of the losses to which it contributes. For example, the most influential parameters at the 10 MW scale are those which affect passage loss because, as seen earlier in Fig. 9, the passage loss is predominant in large turbines. Among the kinematic parameters, the relative flow velocities w_4 and w_5 have the greatest effect. The relative outlet velocity w_5 is more significant because, in addition to passage loss, it affects the trailing edge loss as well. On the other hand, small-scale turbines are penalized more by clearance loss. Therefore, the efficiency is expected to become increasingly sensitive to parameters that contribute to clearance loss as the turbine is scaled down to 0.1 MW. This is confirmed by Fig. 13, in which the significance of terms that appear in Eq. (11), such as ε, U_4, and, Z_r, is amplified in the 0.1 MW turbine. Overall, geometric parameters become more important in 0.1 MW turbines, as observed in the general trend in the right side plot of Fig. 13.

The effect of the physical properties of the fluid, represented by the kinematic viscosity, is the smallest at both scales. Therefore, the differences in the viscosity of the fluids have little sway on turbine performance; in other words, the loss models are fluid-agnostic. It must be emphasized that this conclusion is strictly based on the mathematical nature of the loss models used here, and may not accurately represent the effect that each of these parameters has on the physical flow in the rotor. Indeed, Keep and Jahn [34] conducted a numerical loss investigation of a 300 kW low-specific speed RIT operating with CO_2 and concluded that endwall viscous losses in the stator are more significant than predicted using gas turbine derived preliminary design methods. Moreover,

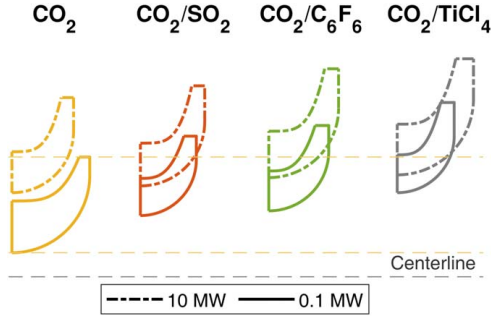

Fig. 14 Rotor meridional profile. Dimensions of 10 MW turbines have been scaled down.

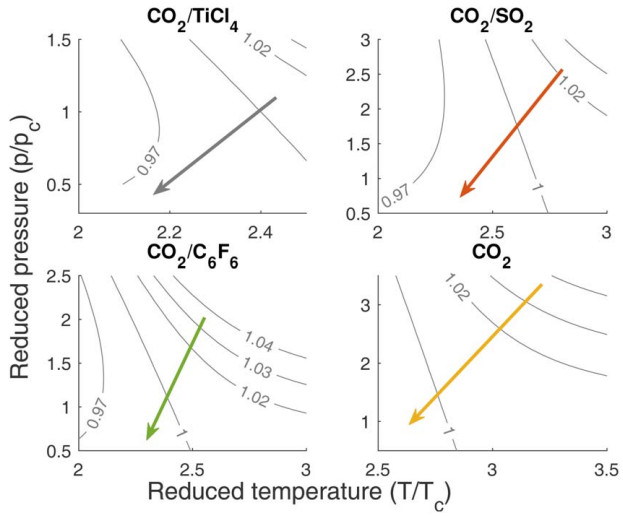

Fig. 15 Expansion process with respect to compressibility contours for 10 MW case B

viscous stresses are stronger at low Reynolds number. Accordingly, losses are likely to have increased sensitivity to the viscosity of the fluid at low Reynolds number, which is not the case here as $Re > 10^6$. However, the trends shown in Fig. 13 justify the convergence of the 1D model on a similar turbine design regardless of the fluid. Ultimately, it's the flow and shape characteristics of a turbine that determine its performance, not the characteristics of the working fluid.

3.4 Similarities and Dissimilarities. The designs of the turbines from case B are compared in Table 5 and Fig. 14. For a given power capacity, the turbines have similar shapes, which may be attributed to the consistency in the design parameters (N_s, ϕ, ψ, ξ, r_5/r_4, r_{5h}/r_{5s}, L_z/b_5). Therefore, a consistent rotor shape optimizes aerodynamic performance regardless of the working fluid. There are a few likely reasons for this. First, all working fluids behave very close to ideal gases throughout the expansion process; they have compressibility factors close to unity. This is confirmed in Fig. 15 where the expansion process with respect to compressibility contours on reduced pressure-temperature axes are depicted. All the working fluids studied here have compressibility values in the range of 0.97 to 1.04 throughout the expansion process. The process shown in Fig. 15 is for 10 MW case B turbines; however, the compressibility factors are within the same range in all cases at all power scales.

Second, the loss models presented in Table 3 mainly depend on kinematic and geometric features of the turbine, which are set by the aforementioned design parameters, and not on the thermophysical properties of the fluid, as explained in Sec. 3.3.

Based on the analysis presented thus far, the differences in turbine performance are attributed to two main aspects: pressure

Downloaded from http://asmedigitalcollection.asme.org/turbomachinery/article-pdf/146/5/051003/7230669/turbo_146_5_051003.pdf by guest on 08 March 2024

Table 8 Parameters assumed fixed in each sub-case for data shown in Fig. 16

Case	p_{04}/p_5	ε/b_4	ν
A1			
A2	X		
A3		X	
A4	X	X	
A5	X	X	X

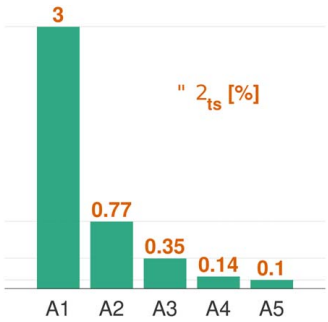

Fig. 16 Difference in efficiency between $CO_2/TiCl_4$ and CO_2 0.1 MW turbines for each sub-case

ratio and clearance-to-height ratio. Fluids which operate in cycles with lower pressure ratios are able to achieve higher turbine efficiencies. Moreover, fluids that have turbines with shorter blades are penalized more by clearance loss. However, as shown in Fig. 11, kinematic viscosity may contribute to the performance differences of the turbines, although slightly.

In the following analysis, case A designs of 0.1 MW $CO_2/TiCl_4$ and CO_2 turbines are revisited to understand the dissimilarities between the fluids by quantifying the influence of pressure ratio, clearance-to-height ratio, and kinematic viscosity. Five sub-cases are devised with a combination of fixed parameters as marked in Table 8. To eliminate the effect of viscosity, a fixed viscosity of 4 mm^2/s was assumed for both fluids in case A5.

According to the results in Fig. 16, the clearance-to-height ratio is the biggest contributor to the difference in performance, followed by the pressure ratio; however, the clearance-to-height ratio will likely be less important in larger turbines. On the other hand, a common viscosity reduces the difference by a mere 0.4%. If pressure ratio, clearance-to-height, and viscosity are all assumed equal, then the difference between the efficiency of the two fluids will be 0.1%, namely due to windage loss differences. A similar analysis at the 10 MW scale yields a difference of 0.05%. Therefore, the uneven performance metrics of the fluids stem from the pressure ratio imposed by the cycle, and by the minimum allowable clearance gap; otherwise, there is no intrinsic aerodynamic advantage of any single mixture over the others.

Doping CO_2 will produce working fluids that are inherently different, despite their ideal gas behavior in the vicinity of the turbine. Although the thermophysical differences do not manifest in different aerodynamic designs, they affect extensive features of the turbine such as size, thrust, torque, and rotational speed.

For a given power capacity and pressure ratio, the level of specific work possible depends on the fluid. Therefore, the mass flow required by the fluids will differ; and so will the size of their respective turbines. Additionally, doping CO_2 changes its density. In the case of the dopants studied here, which were selected to increase the critical temperature, the resulting mixtures have densities that are higher than pure CO_2.

What has been shown thus far is that optimization produces similar turbine designs, in terms of the shape of the rotor and the shape of the velocity diagrams; but the sizes of the turbines will be different, and so will the sizes of their velocity diagrams. For

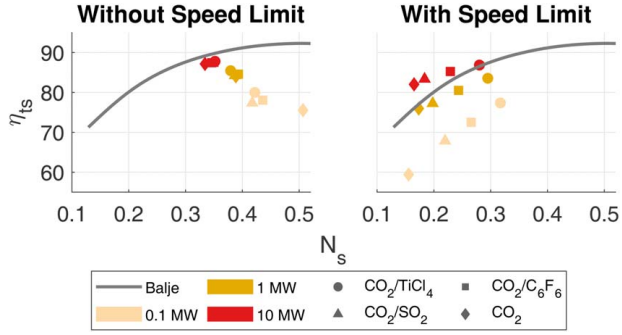

Fig. 17 Specific speed and efficiency comparison of case B with and without a limit of rotational speed

example, owing to its high specific work CO_2/SO_2 turbines have considerably higher tip speeds than the other two mixtures. Likewise, pure CO_2 turbines may have double the rotational speed of $CO_2/TiCl_4$ turbines. Although the consequences on aerodynamic performance are minute, increased rotational speeds entail more demanding bearing selection requirements. Moreover, axial thrust is expected to be greater in turbines with heavier working fluids such as $CO_2/TiCl_4$ or CO_2/C_6F_6, which may alter the thrust balancing requirements depending on the dopant.

Although this study is focused on the aerodynamic characteristics of radial inflow turbines for CO_2-based mixtures, it would be good to discuss some of the mechanical implications of these designs, most potent of which is the rotational speed. An overview of the practical limits of designing CO_2 was presented by Mcclung et al. [35], in which an empirical chart was used to determine the practical rotational speed limit of a generator for a given power output. According to that study, the rotational speed limits for 0.1 MW, 1 MW, and 10 MW turbines are 151 krpm, 46.4 krpm, and 14.3 krpm, respectively. Compared to these limits, the rotational speeds quoted in Table 5 are impractical; for all fluids. The turbines that are the furthest from the practical rotational speed limits are those of CO_2 with rotational speeds about 270% of the speed limit. It is expected that applying the rotational speed limit would penalize the efficiency of all turbines; but to what degree? To answer this question, the optimization in case B is repeated under the aforementioned rotational speed constraints.

Predictably, limiting the rotational speed had a significant influence on the total-to-static efficiency and the specific speeds of the turbines, which are shown in Fig. 17.

The greatest drop in efficiency is 15% for the 0.1 MW CO_2 turbine; the lowest is 1% for the 10 MW $CO_2/TiCl_4$ turbine. Not only does the efficiency drop, but the differences between the turbine designs of the fluids are exacerbated by the practical speed limit, which is notable in the reduction in the specific speed of all designs. The range of specific speeds reduces from $0.3 < N_s < 0.5$; to about $0.15 < N_s < 0.3$;. The restriction of sCO_2 radial inflow turbines to low specific speeds was already noted by Keep [36], and it seems that the same applies to CO_2 mixtures; however, higher specific speeds are possible in mixtures owing to the lower specific work imposed by their cycles. To maintain favorable specific speeds, and thus good efficiency, multi-staging will be required; more so for sCO_2 and SO_2 than for $TiCl_4$ and C_6F_6.

Ultimately, the rotational speed limit is yet another practical limit on turbine design which causes the turbine designs of the fluids to diverge. It is expected that the designs will diverge even further as more design limits are imposed (as was seen with the clearance gap and rotational speed).

4 Conclusion

In this paper, the design of small- to medium-scale radial inflow turbines under multiple design assumptions were analyzed with the aim of discerning the effects of doping CO_2. Results indicate that

Downloaded from http://asmedigitalcollection.asme.org/turbomachinery/article-pdf/146/5/051003/7230669/turbo_146_5_051003.pdf by guest on 08 March 2024

the aerodynamic behavior of the working fluids is similar. Therefore, turbine designs for all working fluids converge on similar rotor shapes and velocity diagrams. However, not all turbines achieve the same performance.

Among the mixtures studied, $CO_2/TiCl_4$ achieved the highest performance, followed by CO_2/C_6F_6, and then CO_2/SO_2. For example, 100 kW turbines for $CO_2/TiCl_4$, CO_2/C_6F_6, CO_2/SO_2, and CO_2 achieve total-to-static efficiencies of 80.0%, 77.4%, 78.1%, and 75.5% respectively. However, the efficiencies for 10 MW turbines are 87.8%, 87.3%, 87.5%, and 87.2%, in the same order.

Variations in the achievable efficiency amongst the fluids stem from variations in their clearance-to-blade height ratio, their pressure ratios, rotational speed limits, and, to a lesser degree, differences in their viscosity. In conclusion, although doping CO_2 has little effect on the aerodynamic performance of the turbine, it is the consequence of the change in cycle conditions along with the design limitations of radial inflow turbines that lead to differences in the performance of the turbines amongst the fluids.

The differences in performance amongst the fluids are greatest in small-scale turbines; with fluids that produce turbines of greater blade heights having the highest efficiency. The effect of clearance loss is attenuated with design optimization by allowing greater flow coefficients, which increase velocities and reduce tip clearance loss. Consequently, the specific speed of the turbines increases at smaller power scales.

The study reveals that loss models are not sensitive to the working fluid. Moreover, the influence of geometric and kinematic parameters changes with power scale. Multi-staging of CO_2, CO_2/SO_2, and CO_2/C_6F_6 turbines is more beneficial than for $CO_2/TiCl_4$ because of the high pressure ratio cycle within which they operate. Additionally, the size of the rotor and the magnitude of the velocities depends on the working fluid, which may entail different mechanical requirements, such as bearing selection and rotordynamics.

It is recommended that future work builds on the findings of this paper by completing a comprehensive mechanical design of the turbines, including bearing selection, rotordynamics, and structural analysis, to ascertain the consequences of doping CO_2 on the full design of the turbine.

Acknowledgment

This work was supported by the European Union's Horizon 2020 research and innovation programme under Grant Agreement No. 814985.

Conflict of Interest

There are no conflicts of interest.

Data Availability Statement

The datasets generated and supporting the findings of this article are obtainable from the corresponding author upon reasonable request.

Nomenclature

h = specific enthalpy (J/kg)
p = pressure (Pa)
t = blade thickness (m)
N = rotational speed (rpm)
T = temperature (K^{-1} or ^oC)
$\dot{m}$ = mass flowrate (kg/s)
Z_n = stator blade count (no)
Z_r = rotor blade count (no)

Greek Symbols

α = absolute flow angle (deg)
β = relative flow angle (deg)
ε = clearance gap height
η = efficiency
ν = kinematic viscosity (mm^2/s)
ξ = meridional velocity ratio
ϕ = flow coefficient
ψ = loading coefficient

Superscripts and Subscripts

h = value at the rotor hub
s = isentropic value
sh = value at the rotor shroud
ts = total-to-static
tt = total-to-total

References

[1] Crespi, F., Arriba, P. R.-d., Sánchez, D., Ayub, A., Marcoberardino, G. D., Invernizzi, C., Martínez, G., Iora, P., Bona, D. D., Binotti, M., and Manzolini, G., 2021, "Thermal Efficiency Gains Enabled by Using Supercritical CO2 Mixtures in Concentrated Solar Power Applications," The 4th European sCO2 Conference for Energy Systems, Virtual Online, Mar. 23–24.
[2] Morosini, E., Ayub, A., di Marcoberardino, G., Invernizzi, C. M., Iora, P., and Manzolini, G., 2022, "Adoption of the CO2 + SO2 Mixture as Working Fluid for Transcritical Cycles: A Thermodynamic Assessment With Optimized Equation of State," Energy Convers. Manage., **255**, p. 115263.
[3] Crespi, F., Rodríguez de Arriba, P., Sánchez, D., and Muñoz, A., 2022, "Preliminary Investigation on the Adoption of CO2-SO2 Working Mixtures in a Transcritical Recompression Cycle," Appl. Therm. Eng., **211**(2021), p. 118384.
[4] Manzolini, G., Binotti, M., Morosini, E., Sanchez, D., Crespi, F., Marcoberdino, G. D., Iora, P., and Invernizzi, C., 2022, "Adoption of CO2 blended With C6F6 as Working Fluid in CSP Plants," p. 090005.
[5] Rodríguez-deArriba, P., Crespi, F., Sánchez, D., Muñoz, A., and Sánchez, T., 2022, "The Potential of Transcritical Cycles Based on CO2 Mixtures: An Exergy-Based Analysis," Renew. Energy, **199**(2), pp. 1606–1628.
[6] Valencia-Chapi, R., Coco-Enríquez, L., and Muñoz-Antón, J., 2020, "Supercritical CO2 Mixtures for Advanced Brayton Power Cycles in Line-Focusing Solar Power Plants," Appl. Sci. (Switzerland), **10**(1), p. 55.
[7] Tafur-escanta, P., Valencia-chapi, R., Ignacio, L., Coco-enr, L., and Muñoz-ant, J., 2021, "Supercritical CO2 Binary Mixtures for Recompression Brayton S-CO2 Power Cycles Coupled to Solar Thermal Energy Plants," Energies., **14**, p. 13.
[8] Valencia-Chapi, R., Coco-Enríquez, L., and Muñoz-Antón, J., 2020, "Comparing Line-Focusing and Central Tower Solar Power Plants With S-CO2 Binary Mixture Brayton Power Cycles," AIP Conf. Proc., **2303**(12), p. 130010.
[9] Valencia-Chapi, R., Tafur-Escanta, P., Coco-Enríquez, L., and Muñoz-Antón, J., 2022, "Supercritical CO2 mixtures for Brayton Power Cycles Complex Configurations With Concentrating Solar Power," AIP Conf. Proc., **2445**(5), p. 090009.
[10] Ma, Y. N., Hu, P., Jia, C. Q., Wu, Z. R., and Chen, Q., 2023, "Thermo-Economic Analysis and Multi-objective Optimization of Supercritical Brayton Cycles With CO2-Based Mixtures," Appl. Therm. Eng., **219**(PA), p. 119492.
[11] Bai, W., Li, H., Zhang, X., Qiao, Y., Zhang, C., Gao, W., and Yao, M., 2022, "Thermodynamic Analysis of CO2–SF6 Mixture Working Fluid Supercritical Brayton Cycle Used for Solar Power Plants," Energy, **261**(PB), p. 124780.
[12] Tang, B., Sun, L., and Xie, Y., 2022, "Design and Performance Evaluation of an Energy Storage System Using CO2-Based Binary Mixtures for Thermal Power Plant Under Dry Conditions," Energy Convers. Manage., **268**(7), p. 116043.
[13] Niu, X., Ma, N., Bu, Z., Hong, W., and Li, H., 2022, "Thermodynamic Analysis of Supercritical Brayton Cycles Using CO2-Based Binary Mixtures for Solar Power Tower System Application," Energy, **254**, p. 124286.
[14] Wang, L., Wang, J., Chen, D., Huang, Y., Sun, W., and Hu, L., 2022, "Investigation on the Effect of Mixtures Physical Properties on Cycle Efficiency in the CO2-Based Binary Mixtures Brayton Cycle," Prog. Nucl. Energy, **143**(10), p. 104049.
[15] Bertini, M., Fiaschi, D., Manfrida, G., Niknam, P. H., and Talluri, L., 2021, "Evaluation of the Property Methods for Pure and Mixture of CO2 for Power Cycles Analysis," Energy Convers. Manage., **245**, p. 114568.
[16] Sun, L., Wang, D., and Xie, Y., 2021, "Thermodynamic and Exergoeconomic Analysis of Combined Supercritical CO2 Cycle and Organic Rankine Cycle Using CO2-Based Binary Mixtures for Gas Turbine Waste Heat Recovery," Energy Convers. Manage., **243**, p. 114400.
[17] Di Marcoberardino, G., Invernizzi, C. M., Iora, P., Ayub, A., Di Bona, D., Chiesa, P., Binotti, M., and Manzolini, G., 2020, "Experimental and Analytical Procedure for the Characterization of Innovative Working Fluids for Power Plants Applications," Appl. Therm. Eng., **178**(5), p. 115513.

Downloaded from http://asmedigitalcollection.asme.org/turbomachinery/article-pdf/146/5/051003/7230669/turbo_146_5_051003.pdf by guest on 08 March 2024

[18] El Samad, T., Teixeira, J. A., and Oakey, J., 2020, "Investigation of a Radial Turbine Design for a Utility-Scale Supercritical CO2 Power Cycle," Appl. Sci. (Switzerland), **10**, p. 4168.
[19] Uusitalo, A., and Grönman, A., 2021, "Analysis of Radial Inflow Turbine Losses Operating With Supercritical Carbon Dioxide," Energies, **14**, p. 3561.
[20] Qi, J., Reddell, T., Qin, K., Hooman, K., and Jahn, I. H., 2017, "Supercritical CO2 Radial Turbine Design Performance as a Function of Turbine Size Parameters," ASME J. Turbomach., **139**(8), p. 081008 .
[21] Zhou, K., Wang, J., Xia, J., Guo, Y., Zhao, P., and Dai, Y., 2020, "Design and Performance Analysis of a Supercritical CO2 Radial Inflow Turbine," Appl. Therm. Eng., **167**(4), p. 114757.
[22] Lv, G., Yang, J., Shao, W., and Wang, X., 2018, "Aerodynamic Design Optimization of Radial-Inflow Turbine in Supercritical CO2 Cycles Using a One-Dimensional Model," Energy Convers. Manage., **165**(5), pp. 827–839.
[23] Persky, R., and Sauret, E., 2019, "Loss Models for On and O Ff -Design Performance of Radial Inflow Turbomachinery," Appl. Therm. Eng., **150**(12), pp. 1066–1077.
[24] Wasserbauer, C. A., and Glassman, A. J., 1975, *Fortran Program for Predicting Off-Design Performance of Radial-Inflow Turbines*, NASA, Cleveland, OH.
[25] Moustapha, H., Zelesky, M. F., Baines, C. N., and Japikse, D., 2003, *Axial and Radial Turbines*, 3rd ed., Concepts ETI Inc, White River Junction, VT.
[26] Ventura, C. A., Jacobs, P. A., Rowlands, A. S., Petrie-Repar, P., and Sauret, E., 2012, "Preliminary Design and Performance Estimation of Radial Inflow Turbines: An Automated Approach," ASME J. Fluids Eng., **134**(3), p. 031102.
[27] Aqel, O., White, M., and Sayma, A., 2021, "Binary Interaction Uncertainty in the Optimisation of a Transcritical Cycle: Consequences on Cycle and Turbine Design," The 4th European sCO2 Conference for Energy Systems, Online Conference, Mar. 23–24, pp. 1–14.
[28] Aungier, R. H., 2006, *Turbine Aerodynamics: Axial Flow and Radial-Inflow Turbine Design and Analysis*, ASME Press, New York.
[29] Whitfield, A., 1990, "Preliminary Design and Performance Prediction Techniques for Centrifugal Compressors," Developments in Industrial Compressors, Vol. 2.
[30] Lee, S., and Gurgenci, H., 2020, "A Comparison of Three Methodological Approaches for Meanline Design of Supercritical CO2 Radial Inflow Turbines," Energy Convers. Manage., **206**(1), p. 112500.
[31] Wright, S. A., Radel, R. F., Vernon, M. E., Rochau, G. E., and Pickard, P. S., 2010, *Operation and Analysis of a Supercritical CO2 Brayton Cycle*, Sandia National Laboratories, Albuquerque, NM.
[32] Aqel, O., White, M., Khader, M., and Sayma, A., 2021, "Sensitivity of Transcritical Cycle and Turbine Design to Dopant Fraction in CO2-Based Working Fluids," Appl. Therm. Eng., **190**, p. 116796.
[33] Baljé, O. E., 1962, "A Study on Design Criteria and Matching of Turbomachines: Part A-Similarity Relations and Design Criteria of Turbines," ASME J. Eng. Gas. Turbines. Power., **84**(1), pp. 83–102.
[34] Keep, J. A., and Jahn, I. H. J., 2019, "Numerical Loss Investigation of a Small Scale, Low Specific Speed Supercritical CO2 Radial Inflow Turbine," ASME J. Eng. Gas Turbines Power, **141**(9), p. 091003.
[35] Mcclung, A., Smith, N., Allison, T., and Tom, B., 2018, "Practical Considerations for the Conceptual Design of an sCO2 cycle," The 6th International Symposium - Supercritical CO2 Power Cycles, San Antonio, TX, Mar. 27–29, pp. 1–21.
[36] Keep, J., 2018, *On the Design of Small to Medium Scale Radial Inflow Turbines for the Supercritical CO_2 Brayton Cycle*, University of Queensland, Brisbane, Australia.
[37] Rodgers, C., 1967, "Efficiency and Performance Characteristics of Radial Turbines," SAE Tech. Pap., **75**(1967), pp. 681–692.
[38] Meroni, A., Robertson, M., Martinez-Botas, R., and Haglind, F., 2018, "A Methodology for the Preliminary Design and Performance Prediction of High-Pressure Ratio Radial-Inflow Turbines," Energy, **164**, pp. 1062–1078.
[39] Daily, J. W., and Nece, R. E., 1960, "Chamber Dimension Effects on Induced Flow and Frictional Resistance of Enclosed Rotating Disks," ASME J. Basic. Eng., **82**(1), pp. 217–230.
[40] White, M. T., 2015, *The Design and Analysis of Radial Inflow Turbines Implemented Within low Temperature Organic Rankine Cycles*, City University of London, London, UK.
[41] Rohlik, H. E., 1968, Analytical Determination of Radial Inflow Turbine Design.
[42] Korpela, S. A., 2019, *Principles of Turbomachinery*, John Wiley & Sons, Hoboken, NJ.

Downloaded from http://asmedigitalcollection.asme.org/turbomachinery/article-pdf/146/5/051003/7230669/turbo_146_5_051003.pdf by guest on 08 March 2024